2023

Simultaneous Measurement of Gas Pressure and Temperature Using a Microbubble Resonator Combined With an FBG

Ketan Dong
Harbin Engineering University, China

Ke Tian
Harbin Engineering University, China

Chuanzhen Zhao
Harbin Engineering University, China

See next page for additional authors

Funder: National Natural Science Foundation of China (NSFC) (62225502, 61935006, 62090062, 62205085); Heilongjiang Provincial Natural Science Foundation of China (LH2020F028); Fundamental Research Funds for the Central Universities (3072022TS2504); 111 Project (B13015); Heilongjiang Touyan Innovation Team Program; Science Foundation Ireland under the Centres research program for the MaREI project (SFI/12/RC/2302_P2)

Simultaneous Measurement of Gas Pressure and Temperature Using a Microbubble Resonator Combined With an FBG

Ketan Dong, Ke Tian, Chuanzhen Zhao, Huibin Li, Jibo Yu, Angzhen Li, Xiaoling Sun, Elfed Lewis, *Senior Member, IEEE*, Gerald Farrell, and Pengfei Wang

***Abstract*—We propose and demonstrate a microbubble resonator combined with a fiber Bragg grating (FBG) for simultaneous measurement of gas pressure and temperature. The approach used allows for very close proximity (<200 μm) between the FBG and the microbubble resonator. The microbubble resonator is fabricated in a section of hollow-core fiber (HCF), spliced to a single-mode fiber (SMF) with a pre-inscribed FBG to form a single-ended open structure. Fresnel reflection from the HCF cleaved end means that broadband light is reflected backwards in the same direction as the Bragg wavelength from the FBG. A tapered fiber couples the reflected broadband light to the microbubble, and both the Bragg peak and whispering gallery modes (WGM) are distinguishable in the signal available for interrogation. The experimental results show that this sensor structure consisting of a microbubble resonator combined with an FBG has the ability to simultaneously measure gas pressure and temperature, while also eliminating temperature crosstalk in gas pressure measurement and providing a useful platform for high accuracy gas pressure detection.**

***Index Terms*—FBG, gas pressure measurement, microbubble resonator, temperature crosstalk, whispering gallery mode.**

Manuscript received 23 April 2023; revised 3 July 2023; accepted 2 August 2023. Date of publication 4 August 2023; date of current version 16 December 2023. This work was supported by the National Natural Science Foundation of China (NSFC) under Grants 62225502, 61935006, 62090062, and 62205085, in part by the Heilongjiang Provincial Natural Science Foundation of China under Grant LH2020F028, in part by the Fundamental Research Funds for the Central Universities under Grant 3072022TS2504, in part by 111 Project to the Harbin Engineering University under Grant B13015, in part by Heilongjiang Touyan Innovation Team Program, and in part by Science Foundation Ireland through Centres Research Program for the MaREI Project under Grant SFI/12/RC/2302_P2. *(Corresponding authors: Ke Tian; Pengfei Wang.)*

Ketan Dong, Ke Tian, Chuanzhen Zhao, Huibin Li, Xiaoling Sun, and Pengfei Wang are with the Key Laboratory of In-fiber Integrated Optics of Ministry of Education, College of Science, Harbin Engineering University, Harbin 150001, China (e-mail: dongketan@hrbeu.edu.cn; ketian@hrbeu.edu.cn; chuanzhenzhao@hrbeu.edu.cn; huibin@hrbeu.edu.cn; xiaolingsun@hrbeu.edu.cn; pengfei.wang@tudublin.ie).

Jibo Yu is with the Xi'an Institute of Applied Optics, Xi'an 710065, China (e-mail: yu20131164@hrbeu.edu.cn).

Angzhen Li is with the College of Science, Tianjin University of Technology, Tianjin 300384, China (e-mail: angzhenli@163.com).

Elfed Lewis is with the Optical Fibre Sensors Research Centre, Department of Electronic and Computer Engineering, University of Limerick, V94 T9PX Limerick, Ireland (e-mail: elfed.lewis@ul.ie).

Gerald Farrell is with the Photonics Research Center, Technological University Dublin, Grangegorman Campus, D07 H6K8 Dublin, Ireland (e-mail: gerald.farrell@tudublin.ie).

Color versions of one or more figures in this article are available at https://doi.org/10.1109/JLT.2023.3302263.

Digital Object Identifier 10.1109/JLT.2023.3302263

I. Introduction

WHISPERING gallery mode (WGM) resonators have attracted a large amount of attention from the research community in both fundamental and applied physics. As a result of their small mode volume and ultrahigh quality (Q) factors, WGM resonators have demonstrated success in a number of areas such as the study of microlasers [1], [2], cavity quantum electrodynamics [3], exceptional points [4], optical frequency combs [5], [6], [7], and optical sensing [8], [9]. A variety of structures have been proposed as WGM resonators, which include the microsphere, microbottle, microbubble, microring, microdisk, microcylinder and microtoroid. Among these various structures, microbubble resonators, which possess a hollow structure with a spherical outer contour, have been shown to possess a diverse range of unique applications such as nanoparticle detection [10], tunable lasers [11], [12], visible comb and supercontinuum generation [13], [14], gas identification and pressure measurement [15], [16].

Microbubble resonators are usually fabricated by means of an arc discharge or by CO_2 laser heating of a pre-tapered capillary tube while simultaneously pressurizing the tube [17], [18]. This method results in the fabricated microbubble cavity which has an ultra-thin wall thickness, which makes it a sensitive gas pressure sensor [15], [19]. However, microbubble-based gas pressure sensors suffer from temperature crosstalk sensitivity, a shortcoming which has not been effectively resolved. This shortcoming reduces the accuracy of gas pressure measurement in practical applications which are subject to temperature fluctuations.

Temperature crosstalk is a common problem in many optical fiber sensors. Accurate measurement of the local temperature, typically using an additional fiber grating, is often used to reduce the effective temperature crosstalk [20], [21]. However, achieving the optimal reduction in temperature crosstalk depends on ensuring very close physical proximity between the optical sensor and the grating in order to avoid any unwanted temperature differential. For microresonator-based optical fibre sensors ensuring close proximity can be a challenge. While many microresonators use a tapered fibre for coupling to and from the resonator, writing a grating in the tapered fiber used for coupling is challenging and reduces the compactness of the device.

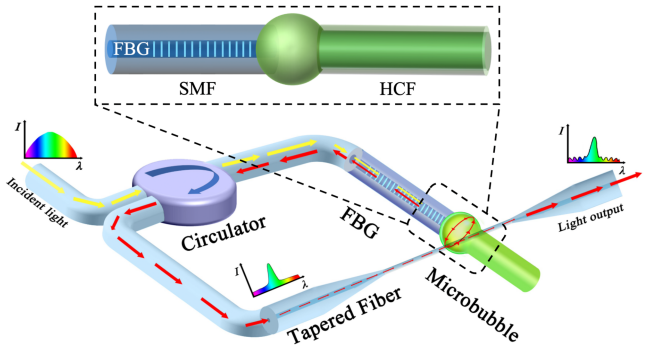

Fig. 1. Schematic diagram of the microbubble resonator combined with an FBG.

In this article, the use of a microbubble resonator combined with an FBG is proposed and demonstrated for simultaneous measurement of gas pressure and temperature. The approach used allows for very close proximity between the FBG and the microbubble resonator (<200 μm), improving compactness and virtually eliminating any risk of unwanted temperature differentials between the FBG and the microbubble resonator. In contrast to the microbubble resonators fabricated in large-diameter capillary tubes, the microbubble resonator in this investigation is created within a hollow core fiber (HCF) which is integrated with a single-mode fiber (SMF) containing a previously inscribed FBG.

II. Principle and Device Fabrication

The schematic diagram of sensing structure is illustrated in Fig. 1, where a single-end open microbubble is spliced to an SMF with an inscribed FBG. In the optical arrangement in Fig. 1, the broadband light is firstly coupled to the FBG through the circulator, with the narrowband light reflected by the FBG returning toward the circulator. The broadband light energy which is not reflected by the FBG reaches the HCF fiber in which the microbubble resonator is fabricated. The end of the HCF is a simple cleaved end at which Fresnel reflection will occur so that broadband light will be reflected backwards toward the circulator.

The FBG reflection and the reflected broadband light are coupled by the circulator into a fiber which is tapered to allow for coupling to and from the microbubble resonator. The optical signal reaching this tapered fiber not only contains the reflected FBG peak but also the broadband light reflected from the end of the HCF. The broadband light coupled to the microbubble resonator results in WGM resonances which manifest themselves as dips in the spectrum at the light output. It is noted that the detected light output not only contains the Bragg reflection peak, which is used to measure temperature, but also spectral dips as a result of WGM resonances which are dependent on the microbubble resonator dimensions and which are influenced by the gas pressure in the microbubble. Thus simultaneous measurement is possible for gas pressure and temperature. Note that a sufficient level of broadband light must reach the tapered fiber if WGMs are to be induced in the microbubble resonator. For this reason, the return loss of the cleaved HCF end was measured and was found to be circa −18 dB, which is found to provide a sufficient level of broadband light to the tapered fiber via the circulator.

The Bragg reflection wavelength λ_{FBG} can be determined by [21]

$$m\lambda_{FBG} = 2n_{eff}\Lambda \tag{1}$$

where m is the order of the Bragg grating, Λ is the grating period, and n_{eff} is the effective refractive index (RI) of the fiber core mode. It is well known that ambient temperature change will cause a shift in the Bragg wavelength.

The WGM resonance wavelength λ_{WGM} can be determined by

$$\lambda_{WGM} = \frac{2\pi n'_{eff} R}{k} \tag{2}$$

where n'_{eff} is the effective RI of the HCF, k represents the azimuth quantum number, and R is the radius of the microbubble at the equatorial plane.

Changes in gas pressure and temperature will cause changes in the effective RI and geometric size of the microbubble resonator, resulting in a shift in the resonance wavelength which can be expressed as [22]

$$\frac{\Delta\lambda_{WGM}}{\lambda_{WGM}} = \frac{\Delta n'_{eff}}{n'_{eff}} + \frac{\Delta R}{R} \tag{3}$$

where $\Delta n'_{eff}$ and ΔR are the effective RI and radius variation of the microbubble resonator, respectively.

When the gas pressure and temperature changes, the resulting wavelength shift of the FBG peak $\Delta\lambda_{FBG}$ and the WGM dip $\Delta\lambda_{WGM}$ can be expressed as follows:

$$\Delta\lambda_{FBG} = K_{T1}\cdot\Delta T + K_{P1}\cdot\Delta P \tag{4}$$

$$\Delta\lambda_{WGM} = K_{T2}\cdot\Delta T + K_{P2}\cdot\Delta P \tag{5}$$

where ΔP and ΔT represent the variations in the gas pressure and temperature. The coefficients K_{P1} and K_{T1} are the sensitivities of the FBG peak shift to gas pressure and temperature, respectively, and K_{P2} and K_{T2} are the sensitivities of the WGM dip shift to gas pressure and temperature, respectively.

The fabrication process for the FBG combined microbubble structure involves a number of steps. Firstly, an FBG with a reflection wavelength at 1549.6 nm was inscribed in a SMF (SMF-28, Corning) using the phase mask method, where the distance of the FBG from the cleaved end of the SMF is about 100 μm. The reason for choosing the phase mask method to write the FBG is to minimize the presence of FBG sidelobes in the reflected broadband light reaching the taper fiber. The subsequent fabrication steps involve the use of a fusion splicer (Fujikura 100P+) as shown in Fig. 2. In Step i, the FBG inscribed SMF and a length of HCF with an inner/outer diameter of 75/125 μm (Polymicro Technologies) were placed in the fiber fusion splicer for alignment. Then in Step ii, the two fibers were spliced, where the discharge current and fusion time for the splicer were set to 10 mA and 400 ms, respectively. It should be noted that the discharge current and time were optimized

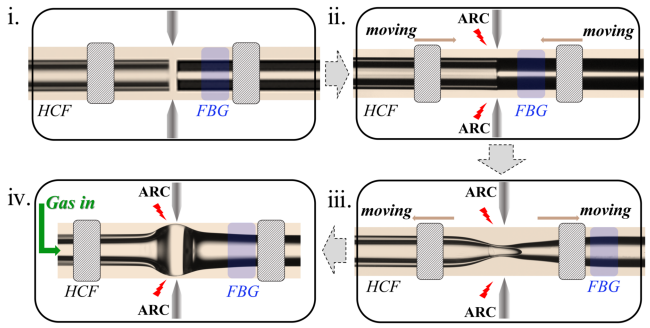

Fig. 2. Schematic of the fabrication process of the FBG combined microbubble structure.

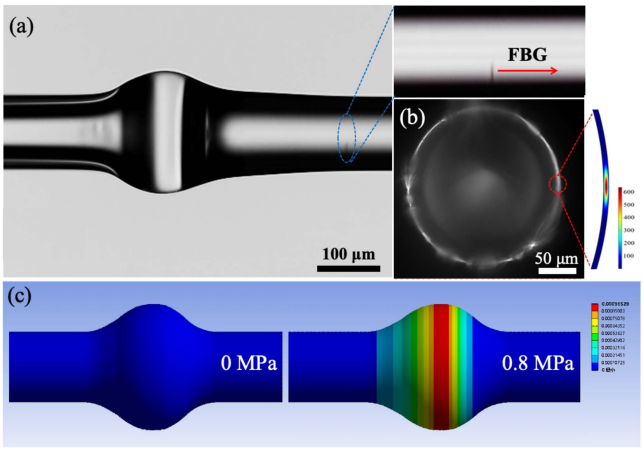

Fig. 3. Microscope images of the fabricated microbubble cavity along (a) side view. Inset: Enlarged view of marker which defines the starting position of the written FBG. (b) View from the end-on direction. Inset: simulated electric field intensity profile for a fundamental mode. (c) Simulated mechanical strain distribution of the microbubble cavity with relative gas pressures of 0 MPa and 0.8 MPa.

to avoid deformation and HCF collapse near the fusion point. In Step iii, the spliced area was moved in the direction of the HCF, so that the electrodes lay about 10 μm from fusion point in Step ii. Then, the fiber holders were moved 160 μm apart, accompanied by an arc discharge. In this way, the HCF was tapered, reducing its diameter while simultaneously reducing its wall thickness. This tapering step is important in the preparation of thin-walled microbubbles, as it not only reduces the wall thickness of the HCF, but also controls the outer diameter of the fabricated microbubble. In Step iv, nitrogen gas was pumped into the open end of the HCF, with an applied gas pressure of 0.016 MPa. The arc was again discharged and under the influence of gas pressure, a microbubble with an equatorial diameter of circa 200 μm was formed in the softened glass. This completed the fabrication of the sensing structure.

The geometric parameters of the fabricated microbubble cavity were measured using an optical microscope (Nikon, LV100N). Fig. 3(a) shows a microscope image of the microbubble cavity from the side while Fig. 3(b) shows an end-on view of the microbubble, viewed along the HCF central axis. The inset in Fig. 3(a) shows the marker written on the outside of the

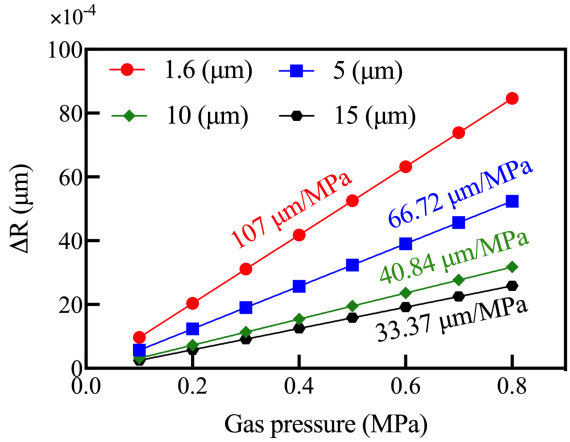

Fig. 4. Simulated gas pressure induced radius variation of microbubbles with wall thicknesses of 1.6 μm, 5 μm, 10 μm, and 15 μm.

fiber using a femtosecond laser (Spectra-Physics), in advance of writing the FBG, which is used to mark the writing start position of the FBG. This marker allows for the spatial distance between the microbubble and FBG to be accurately measured, which is 198 μm. The outer diameter and wall thickness of the microbubble cavity at the equator plane were determined to be 210.2 μm and 1.6 μm, respectively. Based on these geometrical parameters, the electric field intensity profile of the fundamental mode was simulated, as shown in the inset of Fig. 3(b). It is clear that the maximum field intensity lies along the largest (equatorial) diameter region of the microbubble.

In order to study the deformation and strain distribution of the microbubble cavity under the influence of gas pressure, a mechanical analysis was carried out using Ansys software. The Young's modulus, Poisson's ratio, and material density values used in the model are 76.7 GPa, 0.17, and 2.65 g/cm^3, respectively. The geometrical parameters in the model used the measured results above. The wall thicknesses at positions other than the equatorial plane were set to gradually increase in the model from the equatorial plane to the points where the microbubble ends, in effect at the points on the HCF which do not undergo expansion during the formation of the microbubble. Relative gas pressures (that is relative to normal atmospheric pressure) of 0 and 0.8 MPa were applied to the microbubble cavity, and the mechanical strain distribution results are shown in Fig. 3(c). It is clear that when the gas pressure increases, the microbubble cavity strain distribution reaches a maximum value along the equatorial plane, which is the thinnest point in the microbubble wall.

The expansion of microbubbles with increasing gas pressure was also simulated for different wall thicknesses but the same microbubble diameter of 210.2 μm. It can be observed from Fig. 4 that all microbubble cavities undergo expansion with increasing gas pressure. The difference is that for the same gas pressure, the deformation is greater for microbubbles with a thinner wall thickness. The change in the microbubble equatorial diameter will cause a shift in the spectral positions of the WGM dips so that the detection of gas pressure can be

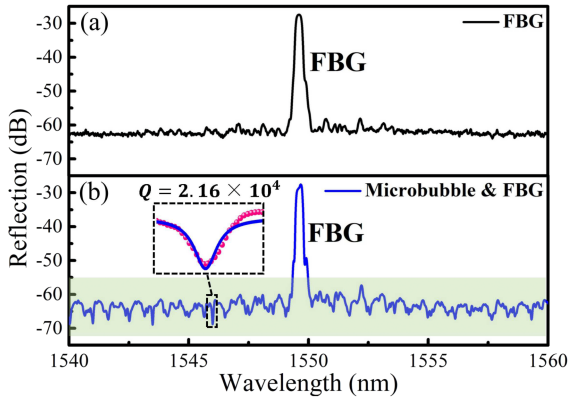

Fig. 5. Measured reflected spectrum of the structure: (a) Without close coupling of the tapered fiber and the microbubble (b) with close coupling of the tapered fiber and the microbubble.

realized using wavelength interrogation. Based on the radius change (ΔR) obtained by simulation and (3), the theoretical gas pressure sensitivities of the microbubble cavity at 1546 nm were calculated, as 163.5 pm/MPa for a 1.6 μm wall thickness, 101.3 pm/MPa for a 5 μm wall thickness, 61.4 pm/MPa for a 10 μm wall thickness, and 50.0 pm/MPa for a 15 μm wall thickness.

Using the experimental setup in Fig. 1, the output spectrum of the complete sensing structure was measured. Fig. 5(a) is the reflection spectrum when the microfiber is not closely coupled with the microbubble resonator. The reflected spectrum in this case is dominated by the Bragg reflection peak. It can also be observed that there are weak sidelobes near the Bragg reflection wavelength, but that as expected, sidelobe levels are almost negligible at positions further from the Bragg reflection wavelength. If the FBG sidelobe levels are too high, there is a risk that they will make it difficult to distinguish and accurately measure spectral shifts in WGM dips. Therefore, it is crucial to choose a suitable FBG fabrication method which will suppress FBG sidelobes to the greatest possible extent. Fig. 5(b) is the reflection spectrum when the microfiber is coupled with the microbubble resonator. The diameter of the microfiber is 1.7 μm, and to ensure the stability of the coupling system, the microfiber is attached to the equatorial plane of the microbubble. It is clear from the presence of spectral dips that WGMs are excited. The signal-to-noise ratio (SNR) can be further improved by increasing the reflectivity of the SMF end-face using a suitable reflection coating and by optimizing the coupling between the microfiber and the microbubble. The Q-factor of the spectral dip at 1546 nm for this microbubble resonator is calculated to be 2.16×10^4 using a Lorentz fit, as shown in the inset in Fig. 5(b). The wavelength dip at 1546 nm was chosen for these calculations as it provides the highest extinction ratio and Q-factor.

III. Experiments and Discussion

Fig. 6 illustrates the experimental setup for gas pressure and temperature measurement. The broadband light provided by a supercontinuum source (SC, YSL) is firstly coupled to the FBG integrated with a microbubble resonator through an optical circulator, and the light signal reflected by the FBG is coupled back to the microfiber-coupled microbubble resonator. Broadband light reflected from the end of the HCF is also coupled back to the microfiber-coupled microbubble resonator. The output light is recorded by an optical spectrum analyzer (OSA, YOKOGAWA AQ6370D). In order to investigate the effect of gas pressure, the single-end open side of the microbubble resonator is connected to a nitrogen cylinder. The applied gas pressure can be adjusted through a valve and the specific pressure value applied is read through a pressure gauge. The whole sensor was placed in an in-house constructed climate-control enclosure which allowed the temperature to be controlled. A digital thermometer was used to monitor the temperature inside the box.

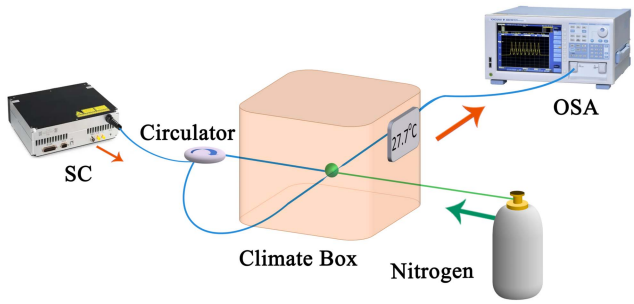

Fig. 6. Experimental setup for gas pressure and temperature sensing test.

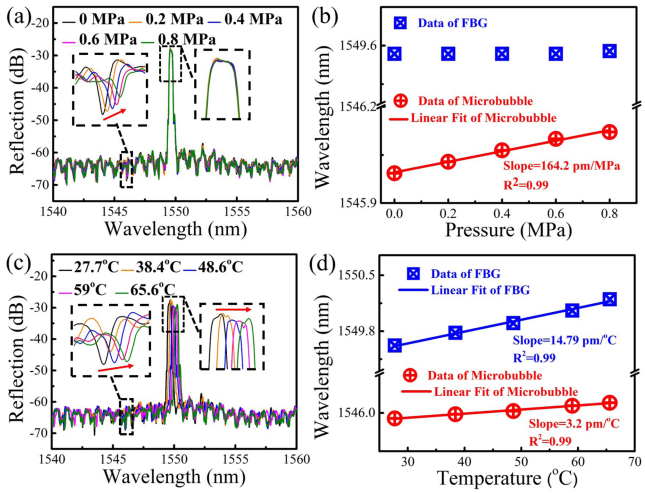

Fig. 7. Spectral evolution of the microbubble resonator combined with an FBG when applied (a) gas pressure increases; (c) temperature increases. Linear fitting as a function of the dip wavelength shift against (b) gas pressure variation; (d) temperature variation.

Fig. 7(a) shows the spectral evolution when the relative gas pressure is increased from 0 to 0.8 MPa in steps of 0.2 MPa. A red-shift can be seen for the WGM spectrum, whereas no discernible shift is observed for the FBG wavelength. This confirms that the FBG reflection wavelength (1549.6 nm) is independent of gas pressure, and its gas pressure sensitivity coefficient in (4) can be denoted as 0. However, in the case of the WGM spectrum, gas pressure variations strongly influence

the resonance wavelength. The spectral shift results for the FBG peak and WGM dip at 1546 nm are plotted in Fig. 7(b) as a function of gas pressure. A linear fit is also shown in Fig. 7(b) for the WGM resonance wavelength dip variation, from which the gas pressure sensitivity was calculated to be 164.2 pm/MPa. This measured gas pressure sensitivity is in good agreement with the simulated value (163.5 pm/MPa). Fig. 7(c) shows the spectral evolution when the temperature was increased from 27.7 °C to 65.6 °C in steps of approximately 10 °C. As the temperature increases, both the WGM transmission spectrum and the FBG wavelength shift to longer wavelengths. The linearly fitted results in Fig. 7(d) show the temperature sensitivities of the WGM dip and the FBG peak are 3.2 pm/°C and 14.79 pm/°C, respectively. The microbubble resonator has a low-temperature sensitivity, which can be attributed to silica's low thermal expansion coefficient of 0.55×10^{-6} /°C. It should also be noted that a lower temperature sensitivity may be attributable to the more efficient heat dissipation of thin-walled microbubbles [17].

The WGM resonance dip wavelength is sensitive to gas pressure and temperature variations, while that of the FBG reflected peak is independent of gas pressure. The combination of the microbubble resonator and the FBG provides for simultaneous measurement of gas pressure and temperature. Based on the measured sensitivity coefficients, a demodulation matrix can be established to determine pressure and temperature values:

$$\begin{bmatrix}\Delta P\\ \Delta T\end{bmatrix} = \begin{bmatrix}0 & 14.79\,\mathrm{pm/^oC}\\ 164.2\,\mathrm{pm/MPa} & 3.2\,\mathrm{pm/^oC}\end{bmatrix}^{-1} \times \begin{bmatrix}\Delta\lambda_{FBG}\\ \Delta\lambda_{WGM}\end{bmatrix} \quad (6)$$

Using the above demodulation matrix, simultaneous measurement of gas pressure and temperature can be realized. A significant advantage of the structure is that, as result of their very close physical proximity, the temperature of the FBG and the microbubble are very closely matched, allowing temperature crosstalk to be virtually eliminated for gas pressure measurement.

IV. Conclusion

In summary, a microbubble resonator combined with an FBG for simultaneous measurement of gas pressure and temperature has been demonstrated. WGM resonance dips and a Bragg peak are present in the received signal, thus allowing for simultaneous measurement. The experimental results show that this sensor structure provides a gas pressure sensitivity of 164.2 pm/MPa and a temperature sensitivity of 14.79 pm/°C. The microbubble resonator combined with an FBG proposed in this investigation eliminates the temperature crosstalk of a microbubble resonator in gas pressure measurement. Furthermore, its compact dimensions offer the potential to develop a complete gas pressure measurement system for use in demanding applications, such as the biomedical area, for example respiratory probes for use during magnetic resonance imaging examinations.

References

[1] P. Wang et al., "Tm^{3+}-doped fluorotellurite glass microsphere resonator laser at 2.3 μm," *Opt. Lett.*, vol. 45, no. 13, pp. 3553–3556, 2020.

[2] B. Jiang, S. Zhu, W. Wang, L. Shi, and X. Zhang, "Room-temperature continuous-wave upconversion white microlaser using a rare-earth-doped microcavity," *Amer. Chem. Soc. Photon.*, vol. 9, no. 9, pp. 2956–2962, 2022.

[3] Y. Louyer, D. Meschede, and A. Rauschenbeutel, "Tunable whispering-gallery-mode resonators for cavity quantum electrodynamics," *Phys. Rev. A*, vol. 72, no. 3, 2005, Art. no. 031801.

[4] C. Wang, W. R. Sweeney, A. D. Stone, and L. Yang, "Coherent perfect absorption at an exceptional point," *Science*, vol. 373, no. 6560, pp. 1261–1265, 2021.

[5] S. H. Lee et al., "Towards visible soliton microcomb generation," *Nature Commun.*, vol. 8, no. 1, 2017, Art. no. 1295.

[6] K. Tian et al., "Blue band nonlinear optics and photodarkening in silica microdevices," *Photon. Res.*, vol. 10, no. 9, pp. 2073–2080, 2022.

[7] F. Lei, Z. Ye, and V. Torres-Company, "Thermal noise reduction in soliton microcombs via laser self-cooling," *Opt. Lett.*, vol. 47, no. 3, pp. 513–516, 2022.

[8] X. Tu et al., "Underwater acoustic wave detection based on packaged optical microbubble resonator," *J. Lightw. Technol.*, vol. 40, no. 18, pp. 6272–6279, Sep. 2022.

[9] D.-Q. Yang et al., "Operando monitoring transition dynamics of responsive polymer using optofluidic microcavities," *Light Sci. Appl.*, vol. 10, no. 1, 2021, Art. no. 128.

[10] J. M. Ward, Y. Yang, F. Lei, X.-C. Yu, Y.-F. Xiao, and S. N. Chormaic, "Nanoparticle sensing beyond evanescent field interaction with a quasi-droplet microcavity," *Optica*, vol. 5, no. 6, pp. 674–677, 2018.

[11] Q. Lu, X. Chen, X. Liu, L. Fu, C.-L. Zou, and S. Xie, "Tunable optofluidic liquid metal core microbubble resonator," *Opt. Exp.*, vol. 28, no. 2, pp. 2201–2209, 2020.

[12] J. Yu et al., "A tellurite glass optical microbubble resonator," *Opt. Exp.*, vol. 28, no. 22, pp. 32858–32868, 2020.

[13] Y. Yang et al., "Four-wave mixing parametric oscillation and frequency comb generation at visible wavelengths in a silica microbubble resonator," *Opt. Lett.*, vol. 41, no. 22, pp. 5266–5269, 2016.

[14] Q. Lu et al., "Optical supercontinuum generation via rotational and vibrational molecular cavity optomechanics," *Laser Photon. Rev.*, vol. 17, no. 2, 2023, Art. no. 2200384.

[15] Y. Yang, S. Saurabh, J. M. Ward, and S. N. Chormaic, "High-Q, ultrathin-walled microbubble resonator for aerostatic pressure sensing," *Opt. Exp.*, vol. 24, no. 1, pp. 294–299, 2016.

[16] Z.-D. Peng, C.-Q. Yu, H.-L. Ren, C.-L. Zou, G.-C. Guo, and C.-H. Dong, "Gas identification in high-Q microbubble resonators," *Opt. Lett.*, vol. 45, no. 16, pp. 4440–4443, 2020.

[17] J. M. Ward, Y. Yang, and S. N. Chormaic, "Highly sensitive temperature measurements with liquid-core microbubble resonators," *IEEE Photon. Technol. Lett.*, vol. 25, no. 23, pp. 2350–2353, Dec. 2013.

[18] S. Berneschi et al., "High Q silica microbubble resonators fabricated by arc discharge," *Opt. Lett.*, vol. 36, no. 17, pp. 3521–3523, 2011.

[19] Q. Lu, J. Liao, S. Liu, X. Wu, L. Liu, and L. Xu, "Precise measurement of micro bubble resonator thickness by internal aerostatic pressure sensing," *Opt. Exp.*, vol. 24, no. 18, pp. 20855–20861, 2016.

[20] K. Tian, G. Farrell, W. Yang, X. Wang, E. Lewis, and P. Wang, "Simultaneous measurement of displacement and temperature based on a balloon-shaped bent SMF structure incorporating an LPG," *J. Lightw. Technol.*, vol. 36, no. 20, pp. 4960–4966, Oct. 2018.

[21] K. Tian et al., "Ultra-compact in-core-parallel-written FBG and Mach-Zehnder interferometer for simultaneous measurement of strain and temperature," *Opt. Lett.*, vol. 46, no. 22, pp. 5595–5598, 2021.

[22] F. Vollmer and S. Arnold, "Whispering-gallery-mode biosensing: Label-free detection down to single molecules," *Nature Methods*, vol. 5, no. 7, pp. 591–596, 2008.